The Journal of Chemical Physics ARTICLE scitation.org/journal/jcp

Comparing zero-parameter theories for the WCA and harmonic-repulsive melting lines

Cite as: J. Chem. Phys. 158, 164504 (2023); doi: 10.1063/5.0147416
Submitted: 22 February 2023 • Accepted: 10 April 2023 •
Published Online: 25 April 2023

Jeppe C. Dyre and Ulf R. Pedersen[a)]

AFFILIATIONS

Glass and Time, IMFUFA, Department of Science and Environment, Roskilde University, P.O. Box 260, DK-4000 Roskilde, Denmark

[a)]Author to whom correspondence should be addressed: ulf@urp.dk

ABSTRACT

The melting line of the Weeks–Chandler–Andersen (WCA) system was recently determined accurately and compared to the predictions of four analytical hard-sphere approximations [Attia *et al.*, J. Chem. Phys. **157**, 034502 (2022)]. Here, we study an alternative zero-parameter prediction based on the isomorph theory, the input of which are properties at a single reference state point on the melting line. The two central assumptions made are that the harmonic-repulsive potential approximates the WCA potential and that pair collisions are uncorrelated. The new approach gives excellent predictions at high temperatures, while the hard-sphere-theory based predictions are better at lower temperatures. Supplementing the WCA investigation, the face-centered-crystal to fluid coexistence line is determined for a system of harmonic-repulsive particles and compared to the zero-parameter theories. The results indicate that the excellent isomorph-theory predictions for the WCA potential at higher temperatures may be partly due to a cancellation of errors between the two above-mentioned assumptions.

I. INTRODUCTION

A central result of classical theories of liquids is that fluid states' structure, dynamics, and statistical properties are determined mainly by their short-ranged repulsive forces, while long-ranged attractions play second fiddle.[1–15] This simplification is behind the success of classical hard-sphere (HS) theories[2,4,5,16,17] and the mapping to a harsh effective inverse power-law pair potential.[18–21] Both approaches predict structure, dynamics, and statistical properties that are functions of a single parameter in the two-dimensional thermodynamic phase diagram. For HS theories, the single parameter is the effective HS packing fraction. Several criteria have been suggested for determining this quantity for a given state point (and model); this is in general a subtle problem, the solution of which *de facto* determines the configurational adiabats of the system in question.[22,23] The oldest approximation for determining the effective HS radius dates back to Boltzmann's thesis,[24] which proposed that the HS diameter is the shortest distance obtained by two particles colliding head-on with average thermal velocity. In the 1960s, Barker and Henderson, Andersen and Weeks and Chandler, and others developed successful theories based on more rigorous thermodynamic arguments.

Since the onset of the present millennium, high-pressure experiments by several groups have established that liquid dynamics is often a function of a single thermodynamic parameter. This has been motivated by mapping to a harsh inverse power-law pair potential.[25,26] The isomorph theory generalizes the idea of an effective single-parameter phase diagram whenever the potential-energy function $U(\mathbf{R})$ obeys hidden scale invariance.[27,28] This is the property that the ordering of configurations according to their potential energy at one density is maintained upon a uniform scaling of all coordinates, expressed in the logical implication $U(\mathbf{R}_a) < U(\mathbf{R}_b) \Rightarrow U(\lambda\mathbf{R}_a) < U(\lambda\mathbf{R}_b)$.[28]

Isomorph theory is exact if the pair interactions are inverse power-law, r^{-n}, in which case the above implication applies for all configurations and structure and dynamic properties are invariant along lines with constant ρ^γ/T, where ρ is density, T is temperature, and $\gamma = n/3$ is the so-called density-scaling exponent. These lines are examples of "isomorphs". It has been shown that numerous systems, such as Lennard-Jones models,[27,29] metals,[21,30] the EXP pair-potential,[31,32] noble elements,[14] and molecular systems,[33–35] have isomorphs to a good approximation. For these systems, the density-scaling exponent is generally state-point dependent, but only weakly so.[36] In contrast, the density-scaling exponent for the

Weeks–Chandler–Andersen (WCA) system diverges when the temperature approaches zero and the system becomes more and more hard-sphere like.[17] Interestingly, isomorph theory still applies in this limit.[17] In Ref. 37, we used the theoretical framework of the isomorph theory to determine the solid–liquid coexistence line of the Lennard-Jones model. Here, we apply this idea to the WCA model and to the model of harmonic-repulsive spheres. While the isomorph theory is mathematically more abstract than the classic HS ideas, it has the advantage of viewing the energy landscape more holistically and avoiding the use of a discontinuous pair potential.

The above-mentioned approaches lead to zero-parameter predictions of the shape of the solid–fluid coexistence line for a given system. Here, we study the harmonic-repulsive[38–45] and the WCA[4,13,14,46–52] pair potentials, both of which approach the hard-sphere potential at low temperatures. We can use any reference state point for the isomorph theory of melting.[37] An attractive possibility that removes this arbitrariness is to use the zero-temperature limit as reference state point, which as shown below results in a theoretical prediction close to that of HS theories. We derive the isomorph-theory prediction for an arbitrary finite-temperature reference state point and compare it to a prediction based on classic HS ideas. While the HS approach gives the best predictions at extremely low temperatures, the isomorph theory is more accurate at the higher temperatures.

We first introduce the two energy surfaces of interest (Sec. II). The low-temperature solid–fluid coexistence line of the WCA system was determined accurately in Ref. 53. In Sec. III, we determine the low-temperature melting line of the harmonic-repulsive system. In Sec. IV, we develop the (zero-parameter) isomorph theory starting from a given reference state point, and in Sec. V, we compare its predictions to those of HS theories. Section VI is a summary. In the Appendix, we derive the temperature dependence of the potential energy at low temperatures.

II. THE WCA AND HARMONIC-REPULSIVE SYSTEMS

We consider two classical systems of repulsive particles. Let $\mathbf{R} = (\mathbf{r}_1, \mathbf{r}_2, \ldots, \mathbf{r}_N)$ be the collective coordinate vector of N particles with mass m confined to the volume V with periodic boundaries; the number density is given by $\rho \equiv N/V$ ($N = 5120$ in all simulations). The total potential energy is a sum of pair-potential contributions,

$$U(\mathbf{R}) = \sum_{i>j}^{N} v(|\mathbf{r}_j - \mathbf{r}_i|). \tag{1}$$

We shall investigate two pair-potentials. The first is the harmonic-repulsive potential defined by

$$v(r) = \varepsilon\left(1 - \frac{r}{\sigma}\right)^2 \quad \text{for } r < \sigma \tag{2}$$

and zero otherwise. Here, ε has the unit of energy and σ has the unit of length. Henceforth, quantities are reported in units derived from m, σ, ε, and the Boltzmann constant k_B. The red line in Fig. 1 shows the harmonic-repulsive pair potential. This potential is often used as a model for colloidal particles, for jamming, and as a component in coarse-grained modeling such as that behind dissipative particle dynamics.[38,40,43–45,54–57]

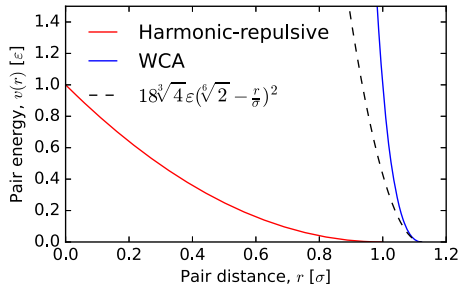

FIG. 1. The harmonic-repulsive (solid red) and WCA (solid blue) pair potentials. The black dashed line is the harmonic-repulsive potential mapped to the same truncation distance and curvature at truncation as the WCA pair potential.

The second system investigated is the WCA pair potential[58,59] defined by

$$v(r) = 4\varepsilon\left[\left(\frac{\sigma}{r}\right)^{12} - \left(\frac{\sigma}{r}\right)^{6}\right] + \varepsilon \quad \text{for } r < r_c \tag{3}$$

and zero otherwise in which

$$r_c = \sqrt[6]{2}\sigma \simeq 1.1225\sigma. \tag{4}$$

The WCA potential is the standard Lennard-Jones potential cut and shifted at its minimum. This implies that the shifted-potential and shifted-force[60] cutoffs are identical. The WCA pair potential was originally introduced as the repulsive reference of the Lennard-Jones system,[8,58] but has since become popular in its own right as a generic fluid model.[16] The blue line in Fig. 1 shows the WCA potential.

At low finite temperatures, it is reasonable to approximate the WCA potential by the first non-vanishing term of a Taylor expansion around $r = r_c$. Thus, one can approximate it as follows (the black dashed line in Fig. 1):

$$v(r) \cong \frac{k_2}{2}(r_c - r)^2 \quad \text{for } r < r_c \tag{5}$$

and zero otherwise in which

$$k_2 \equiv \left.\frac{d^2 v}{dr^2}\right|_{r_c}, \tag{6}$$

yielding $k_2 = 36\sqrt[3]{4}\varepsilon/\sigma^2 \simeq 57\varepsilon/\sigma^2$. Note that Eq. (5) with $k_2 = 2\varepsilon/\sigma^2$ and $r_c = \sigma$ is identical to the harmonic-repulsive pair potential [Eq. (2)]. Thus, the physics of the two models are expected to be equivalent at low temperatures when reported in units derived from k_2 and r_c.

In the $T \to 0$ limit both pair potentials approach that of the hard-sphere (HS) potential corresponding to diameter $d = r_c$,[61–64]

$$v(r) = \infty \quad \text{for } r < d \tag{7}$$

and zero otherwise. In this limit, the effective HS diameter is the truncation distance, $d = r_c$, and the low-temperature solid/liquid coexistence lines approach those of the HS system. The HS coexistence pressure was estimated by Fernández *et al.*[65] to

$$p_d = 11.5712(10)k_BT/d^3, \tag{8}$$

where the value in parenthesis gives the statistical uncertainty on the last digits. Thus, when $T \to 0$ for the harmonic-repulsive system, we expect the coexistence pressure to approach (putting $d = \sigma$)

$$p_\bullet = 11.5712(10)k_BT/\sigma^3, \tag{9}$$

while for the WCA system one gets with $d = \sqrt[6]{2}\sigma$,

$$p_\bullet = 8.1821(7)k_BT/\sigma^3. \tag{10}$$

Throughout this paper, the bullet subscript "•" refers to the HS limit, which the potentials approach when $T \to 0$, i.e., setting $d = r_c$. The fluid and solid densities were estimated by Fernández *et al.*[65] to

$$\rho_d^{(l)} = 0.938\,90(5)/d^3 \tag{11}$$

and

$$\rho_d^{(s)} = 1.037\,15(9)/d^3, \tag{12}$$

respectively. The densities $\rho_\bullet^{(l)}$ and $\rho_\bullet^{(l)}$ are derived by inserting the appropriate d's. Table I lists the constants of the two models.

The effective HS diameter of the harmonic-repulsive and WCA potentials are smaller at finite temperatures. Below we develop and present analytical theories for the shape of the coexistence line when the potentials approach the HS potential.

We note that the WCA and harmonic-repulsive pair-potentials are continuous whereas the HS potential is discontinuous. In effect, some ambiguities are reported in the literature for the latter system regarding higher-order quantities, such as frequency-dependent elastic moduli and transport coefficients.[66–68]

III. THE HARMONIC-REPULSIVE PHASE-TRANSITION LINES AT LOW TEMPERATURES

Recall that the solid/liquid phase transition defines a single line in the thermodynamic pressure–temperature diagram, but two lines and an in-between coexistence region in the density–temperature diagram. The WCA and harmonic-repulsive systems are particularly simple in the sense that they, by being purely repulsive, do not have a gas–liquid phase transition, only a solid–liquid (fluid) transition. The WCA phase-transition line of fluid to face-centered cubic (FCC) crystal was determined accurately in Ref. 53 by combining the interface-pinning method[69–71] and the Gibbs–Duhem integration method[72–74] (the data for the coexistence line are available at http://doi.org/10.5281/zenodo.6505217). In Ref. 53, we investigated four HS approximations for predicting the shape of the WCA melting line. We showed that the Andersen–Weeks–Chandler HS criterion[4] gives the best predictions in the low-temperature limit. In this paper, we extend the analysis to include the predictions of the isomorph theory and study the same problem for the harmonic-repulsive potential.

Zhu *et al.*[75] computed the phase diagram of the single-component harmonic-repulsive system. This system has many crystal structures: FCC, body-centered cubic, base-centered orthorhombic, body-centered tetragonal, diamond crystal structures, and more. The phase diagram also includes several re-entrant melting regions. This richness is similar to that of other ultra-soft potentials such as the Gaussian core,[76] EXP (exponential-repulsive),[77] and Hertzian-sphere pair potentials,[39,42,78–81] which are all characterized by a finite pair potential energy for $r = 0$. We focus here on the low-temperature, low-density part of the phase diagram where the fluid is in equilibrium with an FCC solid. The triple-point temperature between fluid, FCC, and body-centered cubic, is given by $T_{tp} = 0.012\varepsilon/k_B$,[75] which defines the upper limit of the *low-temperature* regime studied in this paper.

To accurately determine the coexistence line below T_{tp}, we combine the interface-pinning method[69] at $T = 0.002\varepsilon/k_B$ with numerical integration of the Clausius–Clapeyron identity.[72–74] The required thermodynamic inputs are estimated from simulations carried out using the leap-frog algorithm with time-step $\Delta t = 0.04\sqrt{m\sigma^2/\varepsilon}$. The pressure and temperature must be constant for the interface-pinning calculations and the Clausius–Clapeyron integration. For this, we use the Langevin-dynamics algorithm of Grønbech–Jensen and Farago[82,83] with a velocity friction coefficient set to $5\varepsilon/\sigma$ and friction coefficient for the simulation-box velocity to $3.67 \times 10^{-7}\varepsilon/\sigma$. The simulations were conducted using the Roskilde University Molecular Dynamics (RUMD) software package version 3.6[84] that utilizes graphics processing units (GPU) for fast computations.

Table II gives the coexistence point determined with the interface-pinning method, and the dots in Fig. 2(a) show the coexistence pressure computed from the integration of the Clausius–Clapeyron identity in temperature steps given by $T_{\text{next}} = T_{\text{previous}}10^{\pm 1/24}$. The dashed line is the theoretical prediction,[53]

$$p(T) = p_\bullet\left(1 + \frac{3\sqrt{\pi}}{2}\tau\right), \tag{13}$$

TABLE I. Constants of models.

	Harmonic-repulsive	WCA
Truncation distance, r_c $[\sigma]$	1	$\sqrt[6]{2}$
Curvature at r_c, k_2 $[\varepsilon/\sigma^2]$	2	$36\sqrt[3]{4}$
HS pressure, $p_\bullet$ $[k_BT/\sigma^3]$	11.571 2(10)	8.182 1(7)
HS solid density, $\rho_\bullet^{(s)}$ $[\sigma^{-3}]$	1.0371 5(9)	0.733 37(6)
HS liquid density, $\rho_\bullet^{(l)}$ $[\sigma^{-3}]$	0.938 90(5)	0.663 90(4)

TABLE II. Coexistence point of the harmonic-repulsive pair potential determined by the interface-pinning method. The numbers in the parenthesis indicate the statistical uncertainty within a 95% confidence interval.

Temperature, T	$0.002\varepsilon/k_B$
Coexistence pressure, p	$0.027\,56(2)\varepsilon/\sigma^3$
Density of solid (FCC), ρ_s	$1.184\,4(3)\sigma^{-3}$
Density of fluid, ρ_l	$1.082\,7(2)\sigma^{-3}$
Volume difference, $\Delta v = \rho_l^{-1} - \rho_s^{-1}$	$0.079\,26(4)\sigma^3$
Entropy of fusion, Δs	$1.227(1)k_B$

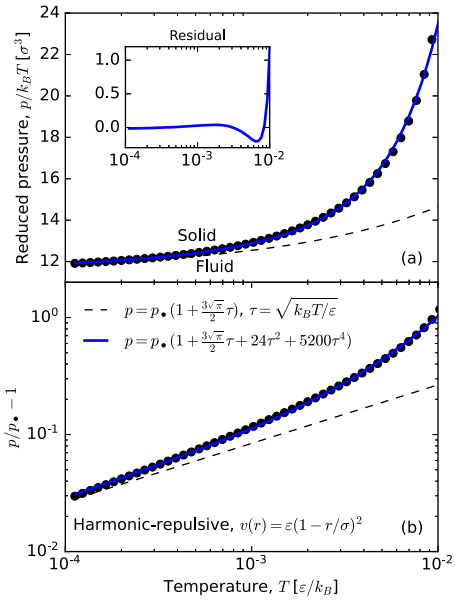

FIG. 2. Solid–fluid coexistence line of the harmonic-repulsive system in the pressure-temperature phase diagram. (a) Dots show the reduced coexistence pressure, p/k_BT, between the fluid and FCC crystal. The black dashed line is the prediction from the HS theory [Eq. (13)] presented in Ref. 53. In this theory, the convergence scales as $T^{\frac{1}{2}}$. The simplest explanation is via Boltzmann's effective HS criterion, $v(d) = k_BT$, where the exponent of two of the pair potential, Eq. (5), is transferred to the two in the $\frac{1}{2}$ of the temperature–scaling exponent. The blue solid line is the empirical fit Eq. (15). The inset shows the residual of the latter. (b) Dots show $p/p_\bullet - 1$ on a logarithmic axis. The black dashed and blue solid lines are the same as in (a).

in which

$$\tau \equiv \sqrt{\frac{k_BT}{\varepsilon}}. \tag{14}$$

In Ref. 53 Eq. (13) is derived for the WCA potential. However, as discussed above, the physics of the WCA and harmonic-repulsive pair potentials are equivalent at low temperatures (and low pressure). Thus the theory applies equally well to the harmonic-repulsive system. The derivation of Eq. (13) is based on the Barker–Henderson[2,5] and Andersen–Weeks–Chandler HS theories,[4,9] which are identical in the low-temperature limit. Equation (13) is arrived at by inserting $k_2 = 2\varepsilon$ and $r_c = \sigma$ into Eqs. (41) and (42) of Ref. 53.

As a testimony to the accuracy of the theory and the computed coexistence line, we note that Eq. (13) gives excellent agreement at low temperatures [compare the black dashed line and dots in Fig. 2(a)]. To highlight the tiny discrepancy, Fig. 2(b) shows the difference in the $T \to 0$ HS prediction, $p_\bullet$, by plotting $p/p_\bullet - 1$ on a logarithmic axis. Even in this representation, the discrepancy is barely visible at the lowest temperatures investigated.

To provide an expression valid also at high temperatures, we fit the coexistence pressure to

$$p(T) = p_\bullet\left(1 + \frac{3\sqrt{\pi}}{2}\tau + a_2\tau^2 + a_4\tau^4\right). \tag{15}$$

By fitting to the data and to the above function represented as $\ln(p/p_\bullet - 1)$, we find $a_2 = 24$ and $a_4 = 5200$. Equation (15) with these parameters is shown as solid blue lines in Figs. 2(a) and 2(b). In Ref. 53, we give a corresponding fit to the WCA coexistence line. We note that Eq. (15) is *not* a theory; it is included here for reference as a practical representation of the coexistence line.

Figure 3(a) shows the density of the face-centered cubic (FCC) solid and fluid at coexistence. The black dashed lines show the above-mentioned HS theory applied to the coexistence density, resulting[53] in

$$\rho_s(T) = \rho_\bullet^{(s)}\left(1 + \frac{3\sqrt{\pi}}{2}\tau\right), \tag{16}$$

and likewise for the fluid density, $\rho_l(T) = \rho_\bullet^{(l)}\left(1 + \frac{3\sqrt{\pi}}{2}\tau\right)$. The solid lines are empirical fits similar to Eq. (15), replacing pressure with density. Figure 3(a) shows $\rho^{(s)}/\rho_\bullet^{(s)} - 1$ and $\rho^{(l)}/\rho_\bullet^{(l)} - 1$ on a logarithmic scale.

IV. ISOMORPH-THEORY PREDICTIONS

Predictions for the thermodynamics of freezing and melting can be made within the framework of isomorph theory.[37] Isomorphs are lines in the phase diagram along which the excess entropy S_{ex}—the entropy in excess of an ideal gas at the same density and temperature—is constant. Such lines always exist, of course, but they are only termed isomorphs if the system obeys hidden scale invariance (Sec. I) to a good approximation, because only in this case are the structure and dynamics predicted to be invariant. Hidden scale

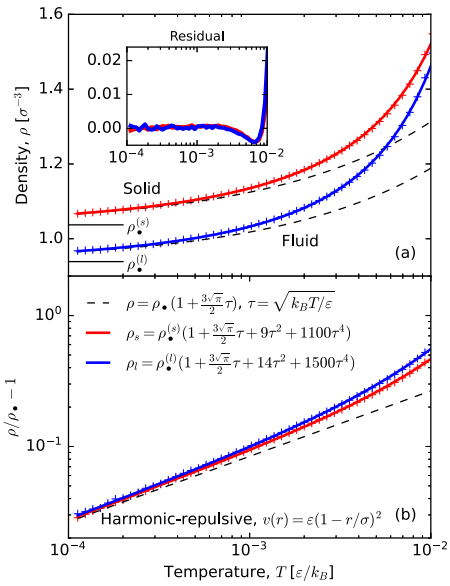

FIG. 3. Solid–fluid coexistence lines of the harmonic-repulsive system in the density–temperature phase diagram. (a) The density of the FCC solid ($\rho = \rho_s$; red +'s) and the fluid ($\rho = \rho_l$; blue +'s) at coexistence. The black dashed lines are the low-temperature analytical predictions of the HS theory presented in Ref. 53. The blue and red solid lines are empirical fits. (b) The same information as in (a) plotted as $\rho/\rho_\bullet - 1$ on a logarithmic scale.

invariance can be checked by evaluating the virial potential-energy correlation coefficient R[27,85] at the relevant state points: if R is close to unity, isomorph theory applies. For more information, we refer the interested reader to Refs. 27, 28, and 86–88; it suffices here to mention that, for instance, the Lennard-Jones, the Yukawa (screened Coulomb), and the EXP system all obey hidden scale invariance and have isomorphs in their liquid and solid phases. Interestingly, it was recently shown that the WCA system has isomorphs throughout its entire phase diagram because the system everywhere obeys $R > \sqrt{8/3\pi} = 0.92$.[17]

In the following, we apply the isomorph theory of freezing[37] to the WCA system.

A. Reference isomorphs

An isomorph can be traced out in the thermodynamic phase diagram by numerical integration in the $\ln T$-$\ln \rho$ plane using, for instance, the classic fourth-order Runge–Kutta method (RK4). At any given state point the required "slope" ("density-scaling exponent") γ is defined by

$$\gamma \equiv \left(\frac{\partial \ln T}{\partial \ln \rho}\right)_{S_{ex}}, \tag{17}$$

which is computed from the virial (W) and potential-energy (U) fluctuations in the NVT ensemble as $\gamma = \langle \Delta W \Delta U \rangle / \langle (\Delta U)^2 \rangle$.[27]

Consider a fluid and a solid isomorph, both touching the coexistence line at the reference state point (p_0, T_0). Specifically, we consider the WCA reference state point

$$T_0 = 0.02\varepsilon/k_B, \tag{18}$$

$$p_0 = 0.175\,23\varepsilon/\sigma^3. \tag{19}$$

Let $u_s(T)$ and $u_l(T)$ be the average potential energy per particle and $\rho_s(T)$ and $\rho_l(T)$ the density along the solid and fluid isomorphs, respectively. The dashed lines in Fig. 4 show these two isomorphs of the WCA fluid (blue) and solid (red), respectively, crossing the coexistence line (solid black) at the reference temperature $T_0 = 0.02\varepsilon/k_B$. The dotted-dashed lines show the isomorphs with reference temperature $T_0 = 2\varepsilon/k_B$. Figure 5 shows the static structure factor, $S(q)$, of the fluid along the freezing line, the fluid isomorph with $T_0 = 2\varepsilon/k_B$, and the $\rho_l = 0.6639\sigma^{-3}$ isochore. The structure is approximately invariant along the freezing line and the isomorph, but not along the isochore. We note that one, in this study, needs to include isomorphs referring to two reference temperatures in order to describe the temperature range of interest. In Ref. 37, we could describe the entire temperature range using a single reference temperature for the Lennard-Jones model. In the present study, we were not able to trace the crystal isomorph with $T_0 = 2\varepsilon/k_B$ below temperatures of $0.05\varepsilon/k_B$ because it moves far into pressures lower than the coexistence pressure (see the red dotted-dashed line in Fig. 4). Thus, we include isomorphs with $T_0 = 0.02\varepsilon/k_B$ for describing the entire temperature range spanning more than four orders of magnitude.

The temperature dependence of the coexistence pressure, $p(T)$, can be found by a Taylor expansion from the isomorphs to where the Gibbs free energy of the two phases are identical.[37] This results in

$$p(T) = p_\star(T)[\alpha_1(T) + \alpha_2(T) + \alpha_3] \tag{20}$$

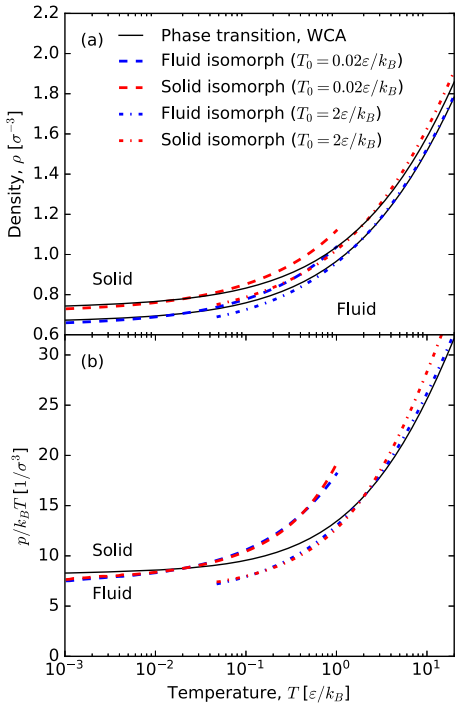

FIG. 4. Isomorphs of the WCA system close to coexistence. (a) shows the fluid–solid coexistence region (enclosed by the solid black lines) in a ρ-T plane, an isomorph of the fluid, and one of the solid (blue and red dashed lines, respectively). The two isomorphs cross the phase transition line at the reference temperature $T_0 = 0.02$. The dotted-dashed lines mark the same for the reference temperature $T_0 = 2$. (b) The same as in the above panel in the (p/k_BT)-T plane.

in which

$$\alpha_1(T) = [u_s(T)/k_BT - u_s(T_0)/k_BT_0] - [u_l(T)/k_BT - u_l(T_0)/k_BT_0], \tag{21}$$

$$\alpha_2(T) = \log(\rho_s(T)/\rho_s(T_0)) - \log(\rho_l(T)/\rho_l(T_0)), \tag{22}$$

$$\alpha_3 = \frac{p_0}{k_BT_0}[\rho_l^{-1}(T_0) - \rho_s^{-1}(T_0)], \tag{23}$$

and

$$p_\star(T) = k_BT/[\rho_l^{-1}(T) - \rho_s^{-1}(T)]. \tag{24}$$

We have here redefined the C's of Ref. 37 and represented the same information in terms of dimensionless α's, introducing $p_\star$ that has the unit of pressure. The dashed lines in Fig. 6 show the empirical value of $p_\star$ and the α's along the $T_0 = 0.02\varepsilon/k_B$ isomorph, and the green dashed line in Fig. 7 shows the prediction of the coexistence line by inserting these into Eq. (20). The prediction is excellent. The red dashed-dotted line in Fig. 7 shows the prediction using the isomorphs with $T_0 = 2\varepsilon/k_B$. Again, the agreement is excellent.

Note that the predictions of the isomorph theory do not involve empirical fitting like Eq. (15), only thermodynamic information along the two isomorphs is required. There is, however, the freedom in picking the coexistence reference-state-point temperature

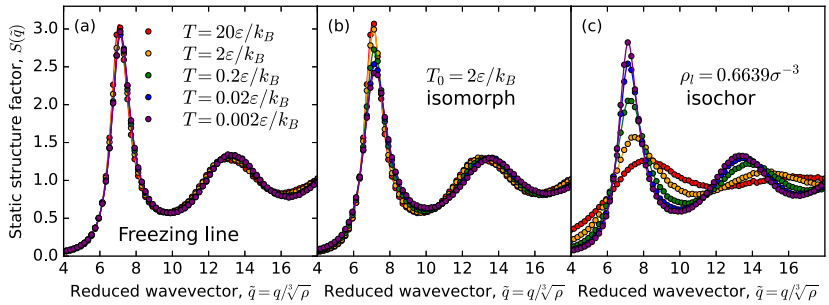

FIG. 5. (a) The static structure factor of the WCA system along the freezing line computed as $S(\mathbf{q}) = \langle|\sum_{n=1}^{N} \exp(\mathrm{i}\mathbf{q}\cdot\mathbf{r}_n)|^2\rangle/N$ where $\mathbf{q} = (0, 0, q)$. The periodic boundary condition dictates that $q = 2\pi n_z/L_z$ where $n_z = 1, 2, \ldots$ and L_z is the length of the box in the z-direction. $S(q)$ is shown as a function of the reduced wavevector, $\tilde{q} = q/\sqrt[3]{\rho}$ (this removes the trivial scaling of the peak positions with density). The dots show $S(\tilde{q})$ at five different state points on the freezing line. The solid lines are cubic splines serving as a guide to the eye. (b) The static structure factor along state points on the isomorph with $T_0 = 2\varepsilon/k$ for the same temperatures as (a). (c) The static structure factor for state points on the $\rho_l = 0.6639\sigma^{-3}$ isochore for the same temperatures as in (a) and (b).

T_0. In the following, we remove this ambiguity by letting $T_0 \to 0$. This results in simple closed forms of Eqs. (20)–(24), giving a good overall description of the coexistence line.

B. Analytical prediction from the isomorph theory

To provide a closed form of Eqs. (20)–(24), we need analytical expressions for the temperature dependence of the potential energy and the density along the fluid and solid isomorphs. We do this by adopting the mean-field approach developed in Ref. 17 (that is exact in infinite dimensions[89]).

First, we investigate when the mean-field approach is appropriate by defining a kissing neighbor as one where the pair distance is shorter than the truncation distance of the pair potential. The solid red line in Fig. 8 shows the relative frequency of particles with none or a single kissing neighbor on the liquid side of the coexistence line. The analysis shows is reasonable to assume that particle collisions are uncorrelated at the lowest temperatures of this study where particles predominantly have none or just a single kissing neighbor.

In general, the partition function for the configurational degrees of freedom is given by $Z = \int_{V^N} d\mathbf{r}_1 \ldots d\mathbf{r}_N \exp\left(-\sum_{i>j} v(r_{ij})/k_BT\right)$. When collisions are uncorrelated, we

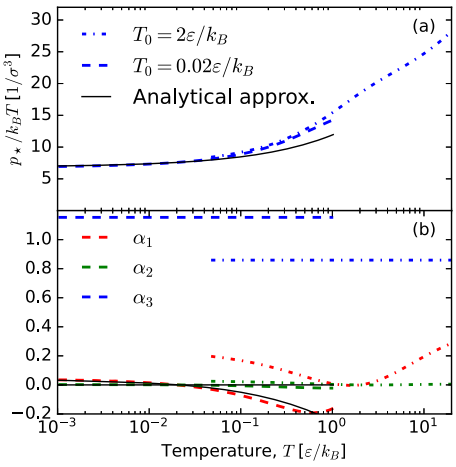

FIG. 6. (a) The blue dashed line shows $p_\star$ [Eq. (24)] evaluated using densities along the solid and fluid isomorphs with $T_0 = 0.02\varepsilon/k_B$ [Fig. 4(a)]. The solid black line is the analytical approximation to $p_\star$ obtained by using the densities given by Eq. (30). The blue dashed-dotted line is $p_\star$ evaluated using the isomorphs with $T_0 = 2\varepsilon/k_B$. (b) The dashed lines show the α's of Eqs. (21)–(23) evaluated using energies and densities of the $T_0 = 0.02\varepsilon/k_B$ isomorphs. The solid lines are analytical approximations arrived at by the insertion of Eqs. (30) and (31) into Eqs. (21)–(23). The dashed–dotted lines are the α's of the $T_0 = 2\varepsilon/k_B$ isomorphs. To a good approximation $|\alpha_2(T)| < |\alpha_1(T)| \ll \alpha_3$, which suggests the approximation $\alpha_1(T) = \alpha_2(T) = 0$.

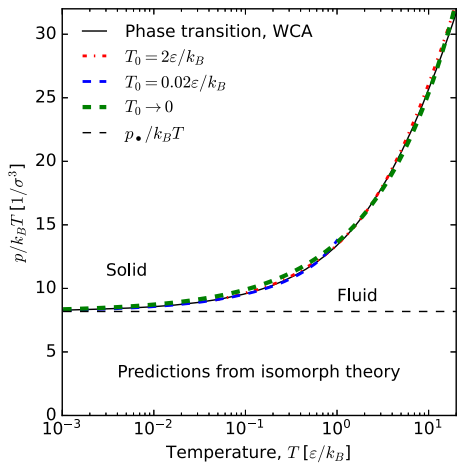

FIG. 7. Zero-parameter predictions (colored dashed lines) for the reduced coexistence pressure (solid black), p/k_BT, based on the isomorph theory. The blue dashed line is Eqs. (20)–(23) evaluated using thermodynamic data of the liquid and solid isomorphs with $T_0 = 0.02\varepsilon/k_B$ shown as dashed lines in Fig. 4. The red dashed-dotted line is constructed using isomorphs with $T_0 = 2\varepsilon/k_B$. The green dashed line is the analytical prediction of Eq. (33) obtained by letting $T_0 \to 0$ in Eqs. (20)–(23). For comparison, the black dashed line is the prediction assuming that WCA particles are HS with diameter equal to the truncation distance, $d = r_c = \sqrt[6]{2}\sigma$.

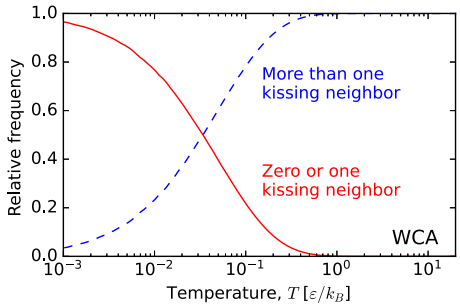

FIG. 8. The solid red line shows the relative fraction of WCA particles with zero or *one kissing* neighbors on the liquid side of the coexistence line, i.e., where the pair distance is shorter than the truncation of the potential, r_c. The dashed blue line shows the relative frequency of particles with more than one kissing neighbor. At low temperatures, it is appropriate to assume uncorrelated particle collisions since the particles here predominantly have have zero or one kissing neighbor.

can treat the interactions in a mean-field way and write the partition function as

$$Z = Z_s^N, \tag{25}$$

where Z_s is the partition function of a single particle moving in the potential $v_s(\mathbf{r})$ of all other particles frozen in space. Z_s has two contributions, one where the moving particle is not kissing and one where it kisses one other particle. The former is the free volume that we will approximate by the entire volume (a low-density approximation), the latter is N times the integral

$$Z_1 = \int_0^{r_c} 4\pi r^2 \exp\left(-v(r)/k_BT\right)dr. \tag{26}$$

Thus, the single-particle partition function can be written as

$$Z_s/N = Z_1 + \rho^{-1}. \tag{27}$$

To evaluate Z_1 [Eq. (26)], we recall that at low temperatures (near the phase transition), WCA particles interact only at distances close to the truncation length r_c, see Eq. (5). With this, we can write Z_1 as a Gaussian integral (see the Appendix).

We now have a mean-field theory for the partition function (Z) that can be used to make predictions of thermodynamic quantities. As an example, in the Appendix, we derive the mean-field prediction of the energy, and in Ref. 17, we show that

$$\gamma \equiv \left.\frac{d\,\log\,T}{d\,\log\,\rho}\right|_{S_{ex}} \tag{28}$$

in the low-temperature limit is given by

$$\gamma(T) = \frac{4r_c\sqrt{2k_2}}{9\sqrt{\pi k_BT}} \quad (T \to 0). \tag{29}$$

By integration of $\gamma(T)$ using $\exp(s) \cong 1 + s$ for $s \to 0$, one finds

$$\rho_l(T) = \rho_l(T_0)\left(1 + \frac{9\sqrt{\pi}[\sqrt{k_BT} - \sqrt{k_BT_0}]}{2r_c\sqrt{2k_2}}\right) \tag{30}$$

and a similar expression for $\rho_s(T)$, in which $\rho_s(T_0) = 0.778963\sigma^{-3}$ and $\rho_l(T_0) = 0.706395\sigma^{-3}$. In the Appendix, we show that the low-temperature limit of the potential energy is proportional to $T^{3/2}$. Thus, using information from the reference state point only, one can write the temperature dependence of the potential energy as

$$u_l(T) = u_l(T_0)[T/T_0]^{3/2} \quad (T \to 0). \tag{31}$$

A similar expression exists for $u_s(T)$, where $u_s(T_0) = 5.512\,03 \times 10^{-3}\varepsilon$ and $u_l(T_0) = 6.337\,50 \times 10^{-3}\varepsilon$.

The solid black lines in Fig. 6 show the analytical approximations of $p_\star$, α_1, and α_2 (α_3 is a constant that does not need to be evaluated). We note that $|\alpha_2(T)| < |\alpha_1(T)| \ll \alpha_3$. Putting $\alpha_1(T) = \alpha_2(T) = 0$, Eqs. (20)–(24) reduce to

$$p(T) = \frac{p_0T}{T_0}\left(1 + \frac{9\sqrt{\pi}[\sqrt{k_BT} - \sqrt{k_BT_0}]}{2r_c\sqrt{2k_2}}\right) \tag{32}$$

after insertion of Eq. (30). The low-temperature HS limit can be used as reference point, i.e., $T_0 \to 0$. Equation (32) then simplifies to

$$p(T) = p_\bullet\left(1 + \frac{9\sqrt{\pi k_BT}}{2r_c\sqrt{2k_2}}\right). \tag{33}$$

This prediction is shown as green dashed lines in Figs. 7 and 9. It compares well to the WCA coexistence line that is shown in solid black. In the following, we will argue, though, that while the agreement is expected at low temperatures, the good overall agreement may result from a fortuitous cancellation of errors of the assumptions at higher temperatures.

For the harmonic-repulsive pair potential, the prediction of the isomorph theory is

$$p(T) = p_\bullet\left(1 + \frac{9\sqrt{\pi}}{4}\tau\right), \tag{34}$$

which is derived by insertion of $k_2 = 2\varepsilon/\sigma^2$ and $r_c = \sigma$ into Eq. (33), where $\tau = \sqrt{k_BT/\varepsilon}$ [Eq. (14)].

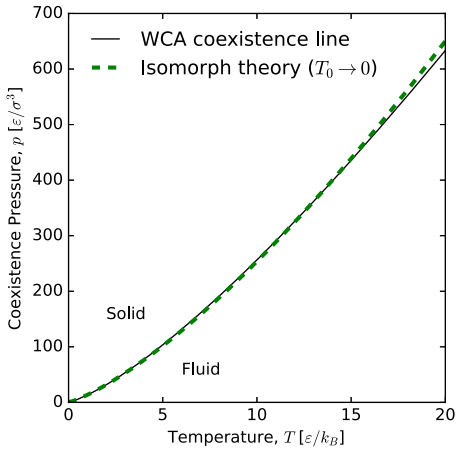

FIG. 9. The isomorph theory's prediction (green dashed line) of the WCA coexistence pressure (solid line).

V. DISCUSSION

We have applied the isomorph theory to predict the shape of the solid–liquid coexistence line. Unlike classical HS theories, this framework does not rely on determining an effective HS diameter. Instead, it uses information along a solid and a liquid isomorph that touches the coexistence line at some reference temperature. The predictions for the WCA coexistence line at high temperatures are significantly better with the isomorph theory than the classic HS theories; compare the red and green dashed lines in Fig. 7 with the HS predictions presented in Ref. 53 (reproduced below). The isomorph-theory prediction depends on the arbitrary reference temperature. If the reference temperature is zero, however, the isomorph theory yields a zero-parameter prediction similar to that of the classic HS theories. Specifically, the green dashed line in Fig. 7 shows that the WCA melting line based on the zero-parameter isomorph theory gives an excellent description over four orders of magnitude in temperature. Two essential assumptions enter into the deviation:

(A) Particle collisions are uncorrelated (Fig. 8).
(B) The WCA potential can be approximated by the harmonic-repulsive potential [Eq. (5); Fig. 1].

Figure 8 shows that the former applies whenever $T < 0.03k_B/\varepsilon$ (pragmatically defined as where the red and blue lines cross in Fig. 8).

To analyze the validity of the latter approximation we conduct a comparative study of the two modes. To this aim, Fig. 10(a) shows the isomorph theory prediction (green dashed) of the harmonic-repulsive melting line (solid black). In the same figure, the red dashed line is the zero-parameter prediction obtained by inserting into Eq. (8) Boltzmann's effective HS criterion[24,53]

$$v(d) = k_BT, \tag{35}$$

leading to

$$d = \sigma(1 - \sqrt{k_BT/\varepsilon}). \tag{36}$$

In the low-temperature limit, the prediction for the coexistence pressure is

$$p(T) = p_\bullet(1 + 3\tau) \quad \text{for } T \to 0. \tag{37}$$

The blue dashed line is the low-temperature HS prediction derived from the Barker–Henderson/Andersen–Weeks–Chandler assumptions [Eq. (13)]. Clearly, all theories underestimate the value of the coexistence pressure at the highest temperatures of this study. We attribute this to errors related to assumption (A), i.e., that particle collisions are uncorrelated.

Figure 10(b) shows the three zero-parameter theories for the WCA melting line. To compare the results of the three theories and two models, Fig. 11 collects all the information of Fig. 10 in a double-logarithmic plot with $2k_BT/k_2r_c^2$ along the abscissa and $p/p_\bullet - 1$ along the ordinate. In this representation, the zero-parameter theories are straight lines with slope 1/2 and the coexistence lines of the two pair-potential collapse at low temperatures. However, the temperatures at which the two models give the same melting line (in reduced units) are rather low, and for higher temperatures, the WCA potential has a lower coexistence pressure since it is harder than the repulsive harmonic potential (compare the solid blue to the black dashed lines in Fig. 1). Moreover, compared to the harmonic-repulsive melting line, the theories predict a lower pressure. As mentioned, this low pressure likely results from the ignored many-body effects, i.e., from the above-mentioned assumption (A). This suggests that the good overall isomorph predictions result in part from a cancellation of assumptions (A) and (B).

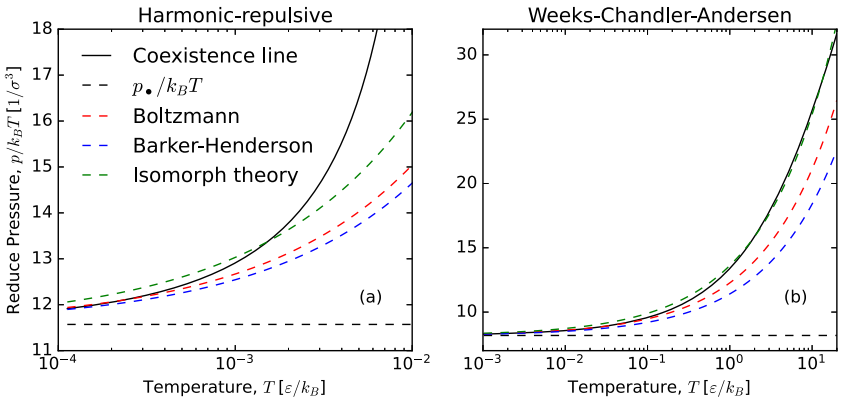

FIG. 10. (a) Comparison of zero-parameter predictions (dashed lines) for the harmonic-repulsive melting line (solid curve). The black dashed line is the zero-temperature limit, where $p_\bullet$ is determined by assuming that the effective HS diameter is equal to the truncation distance $d = r_c = \sigma$ [Eq. (9)]. The red dashed line is obtained from Boltzmann's effective HS diameter[24,53] [Eq. (37)]. The blue dashed line is derived from the classical HS theories[9] of Barker–Henderson[2,5] and Andersen–Weeks–Chandler,[4] which are identical in the zero-temperature limit[53] [Eq. (13)]. The green dashed line is the zero-parameter theory derived in Sec. IV B [Eq. (34)]. (b) Comparison of the three zero-parameter predictions for the shape of the WCA melting line (solid black). The dashed lines are the same as in (a) applied to the WCA system for which $r_c = \sqrt[6]{2}\sigma$ and $k_2 = 36\sqrt[3]{4}\varepsilon/\sigma^3$.

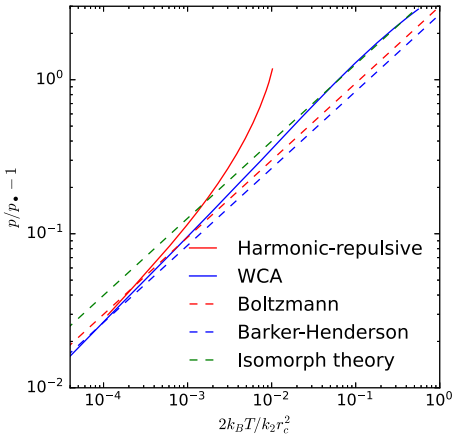

FIG. 11. Comparison of zero-parameter theories (dashed lines) for the harmonic-repulsive (solid red) and WCA (solid blue) melting lines. This figure contains the same information as Fig. 10 represented as $p/p_\bullet - 1$ vs $2k_BT/k_2r_c^2$.

VI. SUMMARY

We have developed an isomorph-theory-based zero-parameter prediction for the melting lines of the harmonic-repulsive and WCA potentials. The new theory generalizes the idea of an effective one-dimensional phase diagram from HS theories without referring to a specific reference potential. The shape of the coexistence line can be evaluated using any of its points as reference state point. We have shown how to generate an analytical prediction using the theory for the shape of the isomorph presented in Ref. 17. Alternatively, we note that Bøhling *et al.*[90] proposed an analytic expression for the shape of the isomorph for any pair-potential, which provides an alternative way to arrive at a closed-form expression of the melting line. We leave this line of prediction for the future.

ACKNOWLEDGMENTS

This work was supported by the VILLUM Foundation's Matter Grant (No. 16515).

AUTHOR DECLARATIONS

Conflict of Interest

The authors have no conflicts to disclose.

Author Contributions

Jeppe C. Dyre: Funding acquisition (lead); Methodology (equal); Writing – review & editing (equal). **Ulf R. Pedersen**: Conceptualization (lead); Data curation (lead); Methodology (equal); Software (lead); Writing – original draft (lead); Writing – review & editing (equal).

DATA AVAILABILITY

The data that support the findings of this study are openly available at http://doi.org/10.5281/zenodo.7646884.

APPENDIX: TEMPERATURE DEPENDENCE OF ENERGY

In the main part of the paper, we use the approximation $u(T) \propto T^{\frac{3}{2}}$ at low temperatures. Here, that approximation is justified.

In Ref. 17, we show that at low densities the low-temperature limit of a pairwise quantity $A(r)$, which is zero for $r > r_c$, has an expectation value that is computed as

$$\langle A \rangle = \frac{1}{Z_s(\rho, T)} \int_0^{r_c} A(r) p(r) dr, \tag{A1}$$

where

$$p(r) = 4\pi r^2 \exp\left[-v(r)/k_BT\right] \tag{A2}$$

is the unnormalized probability,

$$Z_s(\rho, T)/N = Z_1(T) + \frac{1}{\rho} \tag{A3}$$

[see Eq. (27)], and

$$Z_1 = \int_0^{r_c} p(r) dr. \tag{A4}$$

To give an approximation of

$$u(T) = \langle v \rangle \tag{A5}$$

for the pair potential $v(r) = \frac{k_2}{2}(r_c - r)^2$, we need to evaluate integrals of the form

$$\begin{aligned} I_m(T) &= \int_0^{r_c} [v(r)]^m p(r) dr \\ &= \frac{4\pi k_2^m}{2^m} \int_0^{r_c} (r_c - r)^{2m} r^2 \exp\left[-\frac{k_2(r_c - r)^2}{2k_BT}\right] dr. \end{aligned} \tag{A6}$$

From Eq. (A1), the expectation value of the energy per particle ($\langle v \rangle = \langle U \rangle / N$) can be written as

$$\langle v \rangle = \frac{I_1(T)}{I_0(T) + \frac{1}{\rho}}. \tag{A7}$$

By substitution of

$$t = (r_c - r)^2/\tilde{T}, \tag{A8}$$

where

$$\tilde{T} \equiv 2k_BT/k_2, \tag{A9}$$

so $r = r_c - \tilde{T}^{\frac{1}{2}} t^{\frac{1}{2}}$ and $dr = -\frac{1}{2}\tilde{T}^{\frac{1}{2}} t^{-\frac{1}{2}} dt$, we write the integral as

$$\begin{aligned} I_m(T) = \frac{4\pi k_2^m}{2^{m+1}} \int_0^{r_c^2/\tilde{T}} \Big[& r_c^2 \tilde{T}^{m+\frac{1}{2}} t^{m-\frac{1}{2}} + \tilde{T}^{m+\frac{3}{2}} t^{m+\frac{1}{2}} \\ & + 2r_c \tilde{T}^{m+1} t^m \Big] \exp(-t) dt. \end{aligned} \tag{A10}$$

In the low-temperature limit, $\tilde{T} \to 0$, the integral approaches

$$I_m(T) = \frac{4\pi r_c^2 k_2^m}{2^{m+1}} \tilde{T}^{m+\frac{1}{2}} \int_0^\infty t^{m-\frac{1}{2}} \exp(-t) dt. \tag{A11}$$

Thus, the integral of the above approaches the gamma function,

$$\Gamma(z) \equiv \int_0^\infty t^{z-1} \exp(-t) dt, \tag{A12}$$

leading to

$$I_m(T) = \frac{4\pi r_c^2 k_2^m}{2^{m+1}} \tilde{T}^{m+\frac{1}{2}} \Gamma\left(m + \frac{1}{2}\right). \tag{A13}$$

From this, we get

$$I_0(T) = 2\pi r_c^2 \sqrt{\frac{2\pi k_B T}{k_2}} \tag{A14}$$

and

$$I_1(T) = \frac{r_c^2 k_2}{2} \left(\frac{2\pi k_B T}{k_2}\right)^{\frac{3}{2}}. \tag{A15}$$

At low temperatures, the denominator of Eq. (A7) approaches $1/\rho$ since $I_0(T) \propto \sqrt{T}$. The change of ρ in this study is of order 10% while the numerator of Eq. (A7), $I_1(T) \propto T^{\frac{3}{2}}$, changes by orders of magnitude. This justifies the approximation

$$u(T) \propto T^{\frac{3}{2}} \tag{A16}$$

used in the main part of the paper.

REFERENCES

[1] J. D. Bernal, "The Bakerian lecture, 1962. The structure of liquids," Proc. R. Soc. London, Ser. A **280**, 299–322 (1964); available at https://www.jstor.org/stable/2415872.

[2] J. A. Barker and D. Henderson, "Perturbation theory and equation of state for fluids. II. A successful theory of liquids," J. Chem. Phys. **47**, 4714–4721 (1967).

[3] B. Widom, "Intermolecular forces and the nature of the liquid state," Science **157**, 375–382 (1967).

[4] H. C. Andersen, J. D. Weeks, and D. Chandler, "Relationship between the hard-sphere fluid and fluids with realistic repulsive forces," Phys. Rev. A **4**, 1597–1607 (1971).

[5] J. A. Barker and D. Henderson, "What is 'liquid?' Understanding the states of matter," Rev. Mod. Phys. **48**, 587–671 (1976).

[6] D. Chandler, J. D. Weeks, and H. C. Andersen, "Van der Waals picture of liquids, solids, and phase transformations," Science **220**, 787–794 (1983).

[7] L. Berthier and G. Tarjus, "Nonperturbative effect of attractive forces in viscous liquids," Phys. Rev. Lett. **103**, 170601 (2009).

[8] U. R. Pedersen, T. B. Schrøder, and J. C. Dyre, "Repulsive reference potential reproducing the dynamics of a liquid with attractions," Phys. Rev. Lett. **105**, 157801 (2010).

[9] J.-P. Hansen and I. R. McDonald, *Theory of Simple Liquids: With Applications to Soft Matter*, 4th ed. (Academic, New York, 2013).

[10] Z. E. Dell and K. S. Schweizer, "Microscopic theory for the role of attractive forces in the dynamics of supercooled liquids," Phys. Rev. Lett. **115**, 205702 (2015).

[11] J. C. Dyre, "Simple liquids' quasiuniversality and the hard-sphere paradigm," J. Phys. Condens. Matter **28**, 323001 (2016).

[12] J. Chattoraj and M. P. Ciamarra, "Role of attractive forces in the relaxation dynamics of supercooled liquids," Phys. Rev. Lett. **124**, 028001 (2020).

[13] M. K. Nandi and S. M. Bhattacharyya, "Microscopic theory of softness in supercooled liquids," Phys. Rev. Lett. **126**, 208001 (2021).

[14] A. Singh and Y. Singh, "How attractive and repulsive interactions affect structure ordering and dynamics of glass-forming liquids," Phys. Rev. E **103**, 052105 (2021).

[15] S. Toxvaerd, "Role of the attractive forces in a supercooled liquid," Phys. Rev. E **103**, 022611 (2021).

[16] D. M. Heyes and H. Okumura, "Equation of state and structural properties of the Weeks–Chandler–Andersen fluid," J. Chem. Phys. **124**, 164507 (2006).

[17] E. Attia, J. C. Dyre, and U. R. Pedersen, "Extreme case of density scaling: The Weeks–Chandler–Andersen system at low temperatures," Phys. Rev. E **103**, 062140 (2021).

[18] W. G. Hoover, S. G. Gray, and K. W. Johnson, "Thermodynamic properties of the fluid and solid phases for inverse power potentials," J. Chem. Phys. **55**, 1128–1136 (1971).

[19] S. M. Stishov, "The thermodynamics of melting of simple substances," Sov. Phys. Usp. **17**, 625–643 (1975).

[20] D. A. Young, "Soft-sphere model for liquid metals," Tech. Rep., Lawrence Livermore National Lab. (LLNL), Livermore, CA, 1977.

[21] F. Hummel, G. Kresse, J. C. Dyre, and U. R. Pedersen, "Hidden scale invariance of metals," Phys. Rev. B **92**, 174116 (2015).

[22] Y. Rosenfeld, "Relation between the transport coefficients and the internal entropy of simple systems," Phys. Rev. A **15**, 2545–2549 (1977).

[23] Y. Rosenfeld, "A quasi-universal scaling law for atomic transport in simple fluids," J. Phys.: Condens. Matter **11**, 5415–5427 (1999).

[24] L. Boltzmann, *Lectures on Gas Theory* (Dover Publications, 1864).

[25] C. M. Roland, S. Hensel-Bielowka, M. Paluch, and R. Casalini, "Supercooled dynamics of glass-forming liquids and polymers under hydrostatic pressure," Rep. Prog. Phys. **68**, 1405–1478 (2005).

[26] D. Gundermann, U. R. Pedersen, T. Hecksher, N. P. Bailey, B. Jakobsen, T. Christensen, N. B. Olsen, T. B. Schrøder, D. Fragiadakis, R. Casalini, C. Michael Roland, J. C. Dyre, and K. Niss, "Predicting the density-scaling exponent of a glass-forming liquid from Prigogine–Defay ratio measurements," Nat. Phys. **7**, 816–821 (2011).

[27] N. Gnan, T. B. Schrøder, U. R. Pedersen, N. P. Bailey, and J. C. Dyre, "Pressure-energy correlations in liquids. IV. 'Isomorphs' in liquid phase diagrams," J. Chem. Phys. **131**, 234504 (2009).

[28] T. B. Schrøder and J. C. Dyre, "Simplicity of condensed matter at its core: Generic definition of a Roskilde-simple system," J. Chem. Phys. **141**, 204502 (2014).

[29] T. B. Schrøder, N. Gnan, U. R. Pedersen, N. P. Bailey, and J. C. Dyre, "Pressure-energy correlations in liquids. V. Isomorphs in generalized Lennard-Jones systems," J. Chem. Phys. **134**, 164505 (2011).

[30] L. Friedeheim, N. P. Bailey, and J. C. Dyre, "Effectively one-dimensional phase diagram of CuZr liquids and glasses," Phys. Rev. B **103**, 134204 (2021).

[31] A. K. Bacher, T. B. Schrøder, and J. C. Dyre, "The EXP pair-potential system. II. Fluid phase isomorphs," J. Chem. Phys. **149**, 114502 (2018).

[32] A. K. Bacher, U. R. Pedersen, T. B. Schrøder, and J. C. Dyre, "The EXP pair-potential system. IV. Isotherms, isochores, and isomorphs in the two crystalline phases," J. Chem. Phys. **152**, 094505 (2020).

[33] H. W. Hansen, F. Lundin, K. Adrjanowicz, B. Frick, A. Matic, and K. Niss, "Density scaling of structure and dynamics of an ionic liquid," Phys. Chem. Chem. Phys. **22**, 14169–14176 (2020).

[34] S. Mehri, J. C. Dyre, and T. S. Ingebrigtsen, "Hidden scale invariance in the Gay–Berne model," Phys. Rev. E **105**, 064703 (2022).

[35] E. Attia, J. C. Dyre, and U. R. Pedersen, "Isomorph invariance in the liquid and plastic-crystal phases of asymmetric-dumbbell models," Fluids **2**, 388–403 (2022).

[36] A. Sanz, T. Hecksher, H. W. Hansen, J. C. Dyre, K. Niss, and U. R. Pedersen, "Experimental evidence for a state-point-dependent density-scaling exponent of liquid dynamics," Phys. Rev. Lett. **122**, 055501 (2019).

[37]U. R. Pedersen, L. Costigliola, N. P. Bailey, T. B. Schrøder, and J. C. Dyre, "Thermodynamics of freezing and melting," Nat. Commun. **7**, 12386 (2016).
[38]Y.-L. Zhu and Z.-Y. Lu, "Phase diagram of spherical particles interacted with harmonic repulsions," J. Chem. Phys. **134**, 044903 (2011).
[39]P. S. Mohanty, D. Paloli, J. J. Crassous, E. Zaccarelli, and P. Schurtenberger, "Effective interactions between soft-repulsive colloids: Experiments, theory, and simulations," J. Chem. Phys. **140**, 094901 (2014).
[40]V. A. Levashov, "Crystalline structures of particles interacting through the harmonic-repulsive pair potential," J. Chem. Phys. **147**, 114503 (2017).
[41]N. Xu, "Phase behaviors of soft-core particle systems," Chin. J. Polym. Sci. **37**, 1065–1082 (2019).
[42]A. Martín-Molina and M. Quesada-Pérez, "A review of coarse-grained simulations of nanogel and microgel particles," J. Mol. Liq. **280**, 374–381 (2019).
[43]V. A. Levashov, R. Ryltsev, and N. Chtchelkatchev, "Anomalous behavior and structure of a liquid of particles interacting through the harmonic-repulsive pair potential near the crystallization transition," Soft Matter **15**, 8840–8854 (2019).
[44]V. A. Levashov, R. E. Ryltsev, and N. M. Chtchelkatchev, "Structure of the simple harmonic-repulsive system in liquid and glassy states studied by the triple correlation function," J. Condens. Matter Phys. **33**, 025403 (2020).
[45]K. P. Santo and A. V. Neimark, "Dissipative particle dynamics simulations in colloid and interface science: A review," Adv. Colloid Interface Sci. **298**, 102545 (2021).
[46]A. Eskandari Nasrabad, "Thermodynamic and transport properties of the Weeks–Chandler–Andersen fluid: Theory and computer simulation," J. Chem. Phys. **129**, 244508 (2008).
[47]A. Ahmed and R. J. Sadus, "Phase diagram of the Weeks–Chandler–Andersen potential from very low to high temperatures and pressures," Phys. Rev. E **80**, 061101 (2009).
[48]D. Ben-Amotz and G. Stell, "Reformulation of Weeks–Chandler–Andersen perturbation theory directly in terms of a hard-sphere reference system," J. Phys. Chem. B **108**, 6877–6882 (2004).
[49]R. Benjamin and J. Horbach, "Crystal growth kinetics in Lennard-Jones and Weeks–Chandler–Andersen systems along the solid–liquid coexistence line," J. Chem. Phys. **143**, 014702 (2015).
[50]L.-C. Valdès, J. Gerges, T. Mizuguchi, and F. Affouard, "Crystallization tendencies of modelled Lennard-Jones liquids with different attractions," J. Chem. Phys. **148**, 014501 (2018).
[51]A. Banerjee and D. J. Wales, "Energy landscapes for a modified repulsive Weeks–Chandler–Andersen potential," J. Condens. Matter Phys. **34**, 034004 (2021).
[52]Y. Zhou, B. Mei, and K. S. Schweizer, "Activated relaxation in supercooled monodisperse atomic and polymeric WCA fluids: Simulation and ECNLE theory," J. Chem. Phys. **156**, 114901 (2022).
[53]E. Attia, J. C. Dyre, and U. R. Pedersen, "Comparing four hard-sphere approximations for the low-temperature WCA melting line," J. Chem. Phys. **157**, 034502 (2022).
[54]P. J. Hoogerbrugge and J. M. V. A. Koelman, "Simulating microscopic hydrodynamic phenomena with dissipative particle dynamics," Europhys. Lett. **19**, 155 (1992).
[55]R. D. Groot and P. B. Warren, "Dissipative particle dynamics: Bridging the gap between atomistic and mesoscopic simulation," J. Chem. Phys. **107**, 4423–4435 (1997).
[56]C. S. O'Hern, L. E. Silbert, A. J. Liu, and S. R. Nagel, "Jamming at zero temperature and zero applied stress: The epitome of disorder," Phys. Rev. E **68**, 011306 (2003).
[57]P. Español and P. B. Warren, "Perspective: Dissipative particle dynamics," J. Chem. Phys. **146**, 150901 (2017).
[58]J. D. Weeks, D. Chandler, and H. C. Andersen, "Role of repulsive forces in determining the equilibrium structure of simple liquids," J. Chem. Phys. **54**, 5237–5247 (1971).
[59]Y. Zhou, B. Mei, and K. S. Schweizer, "Integral equation theory of thermodynamics, pair structure, and growing static length scale in metastable hard sphere and Weeks–Chandler–Andersen fluids," Phys. Rev. E **101**, 042121 (2020).
[60]S. Toxvaerd and J. C. Dyre, "Communication: Shifted forces in molecular dynamics," J. Chem. Phys. **134**, 081102 (2011).
[61]B. J. Alder and T. E. Wainwright, "Phase transition for a hard sphere system," J. Chem. Phys. **27**, 1208–1209 (1957).
[62]W. W. Wood and J. D. Jacobson, "Preliminary results from a recalculation of the Monte Carlo equation of state of hard spheres," J. Chem. Phys. **27**, 1207–1208 (1957).
[63]B. J. Alder and T. E. Wainwright, "Studies in molecular dynamics. I. General method," J. Chem. Phys. **31**, 459–466 (1959).
[64]B. J. Alder and T. E. Wainwright, "Studies in molecular dynamics. II. Behavior of a small number of elastic spheres," J. Chem. Phys. **33**, 1439–1451 (1960).
[65]L. A. Fernández, V. Martín-Mayor, B. Seoane, and P. Verrocchio, "Equilibrium fluid-solid coexistence of hard spheres," Phys. Rev. Lett. **108**, 165701 (2012).
[66]J. W. Dufty, "Stress tensor and elastic properties for hard and soft spheres," Granul. Matter **14**, 271–275 (2011).
[67]S. Khrapak, "Elastic properties of dense hard-sphere fluids," Phys. Rev. E **100**, 032138 (2019).
[68]S. Khrapak, N. P. Kryuchkov, L. A. Mistryukova, and S. O. Yurchenko, "From soft- to hard-sphere fluids: Crossover evidenced by high-frequency elastic moduli," Phys. Rev. E **103**, 052117 (2021).
[69]U. R. Pedersen, "Direct calculation of the solid–liquid Gibbs free energy difference in a single equilibrium simulation," J. Chem. Phys. **139**, 104102 (2013).
[70]U. R. Pedersen, F. Hummel, G. Kresse, G. Kahl, and C. Dellago, "Computing Gibbs free energy differences by interface pinning," Phys. Rev. B **88**, 094101 (2013).
[71]U. R. Pedersen, F. Hummel, and C. Dellago, "Computing the crystal growth rate by the interface pinning method," J. Chem. Phys. **142**, 044104 (2015).
[72]D. A. Kofke, "Gibbs–Duhem integration: A new method for direct evaluation of phase coexistence by molecular simulation," Mol. Phys. **78**, 1331–1336 (1993).
[73]D. A. Kofke, "Direct evaluation of phase coexistence by molecular simulation via integration along the saturation line," J. Chem. Phys. **98**, 4149–4162 (1993).
[74]D. Frenkel and B. Smit, *Understanding Molecular Simulation : From Algorithms to Applications*, 2nd ed. (Academic Press, San Diego, 2002).
[75]L.-F. Zhu, J. Janssen, S. Ishibashi, F. Körmann, B. Grabowski, and J. Neugebauer, "A fully automated approach to calculate the melting temperature of elemental crystals," Comput. Mater. Sci. **187**, 110065 (2021).
[76]F. H. Stillinger, "Phase transitions in the Gaussian core system," J. Chem. Phys. **65**, 3968–3974 (1976).
[77]U. R. Pedersen, A. K. Bacher, T. B. Schrøder, and J. C. Dyre, "The EXP pair-potential system. III. Thermodynamic phase diagram," J. Chem. Phys. **150**, 174501 (2019).
[78]J. C. Pàmies, A. Cacciuto, and D. Frenkel, "Phase diagram of Hertzian spheres," J. Chem. Phys. **131**, 044514 (2009).
[79]W. Ouyang, C. Fu, Z. Sun, and S. Xu, "Polymorph selection and nucleation pathway in the crystallization of Hertzian spheres," Phys. Rev. E **94**, 042805 (2016).
[80]L. Athanasopoulou and P. Ziherl, "Phase diagram of elastic spheres," Soft Matter **13**, 1463–1471 (2017).
[81]G. Munaò and F. Saija, "Monte Carlo simulation and integral equation study of Hertzian spheres in the low-temperature regime," J. Chem. Phys. **151**, 134901 (2019).
[82]N. Grønbech-Jensen and O. Farago, "Constant pressure and temperature discrete-time Langevin molecular dynamics," J. Chem. Phys. **141**, 194108 (2014).

[83]N. Grønbech-Jensen, N. Robert Hayre, and O. Farago, "Application of the G-JF discrete-time thermostat for fast and accurate molecular simulations," Comput. Phys. Commun. **185**, 524–527 (2014).
[84]N. Bailey, T. Ingebrigtsen, J. S. Hansen, A. Veldhorst, L. Bøhling, C. Lemarchand, A. Olsen, A. Bacher, L. Costigliola, U. R. Pedersen, H. Larsen, J. C. Dyre, and T. B. Schrøder, "RUMD: A general purpose molecular dynamics package optimized to utilize GPU hardware down to a few thousand particles," SciPost Phys. **3**, 038 (2017).
[85]U. R. Pedersen, N. P. Bailey, T. B. Schrøder, and J. C. Dyre, "Strong pressure-energy correlations in van der Waals liquids," Phys. Rev. Lett. **100**, 015701 (2008).
[86]N. P. Bailey, U. R. Pedersen, N. Gnan, T. B. Schrøder, and J. C. Dyre, "Pressure-energy correlations in liquids. I. Results from computer simulations," J. Chem. Phys. **129**, 184507 (2008).
[87]J. C. Dyre, "Hidden scale invariance in condensed matter," J. Phys. Chem. B **118**, 10007–10024 (2014).
[88]J. C. Dyre, "Isomorph theory of physical aging," J. Chem. Phys. **148**, 154502 (2018).
[89]T. Maimbourg and J. Kurchan, "Approximate scale invariance in particle systems: A large-dimensional justification," Europhys. Lett. **114**, 60002 (2016).
[90]L. Bøhling, N. P. Bailey, T. B. Schrøder, and J. C. Dyre, "Estimating the density-scaling exponent of a monatomic liquid from its pair potential," J. Chem. Phys. **140**, 124510 (2014).